Comparison of the Corrosion Behavior of High Strength Aluminum Alloys after Exposure to ASTM B117 Environment

S.N. Grieshop*, R.G. Buchheit*

*Ohio State University, Department of Materials Science and Engineering, 477 Watts Hall, Columbus, OH.

Abstract

In recent years, design requirements for new aircraft have required materials engineers to develop a stronger yet lighter aluminum alloy than the traditional AA7075 and AA2024 type alloys used previously. The aluminum-lithium alloy system is attractive to the aerospace industry due to the its lower density, increased elastic modulus, increased fatigue crack growth resistance, formation of strengthening phases, and increased corrosion resistance when compared to AA7075 and AA2024. Third generation aluminum-lithium alloys have proven to be a viable replacement for incumbent alloys AA7075 and AA2024 in aircraft structures. A key interest in these alloys is increased corrosion resistance and much research has been done to understand the corrosion mechanisms present in 3rd generation aluminum-lithium. Despite this, no direct comparison of the bulk corrosion behavior observed in AA7075 to that observed in a 3rd generation aluminum-lithium alloy, like AA2099, has been reported. To this end, B117 salt fog exposure tests were performed on AA7075, AA7050, AA2099, and AA2024 plate samples, in the longitudinal (L), short transverse (ST), and longitudinal transverse (LT) directions, to compare their corrosion behavior. AA2524 sheet alloy was also compared in the longitudinal direction. Three tests were performed, an interrupted test of 72 hours, 120 hours, and a longer duration 168 hours test, with analysis of the results performed by optical microscopy, optical profilometry, and scanning electron microscopy**.** Optical microscopy of the AA7075, AA7050, and AA2024 samples generally showed localized shallow pitting with trenching around some secondary phase particles as well as areas of localized corrosion on the ST and LT directions. In contrast, AA2099

samples featured small pits across the sample surface with no evidence of trenching due to the alloys lack of secondary particles. Localized corrosion was not observed in the AA2099 samples at all exposure conditions. Analysis of the interrupted test samples by optical profilometry reveals that for a lower limit threshold of 20.0 microns and an upper limit threshold of 1500 microns, AA7075 and AA2024 featured more pits than the longitudinal, short-transverse, and longitudinal-transverse directions of AA2099. AA7075, AA7050, AA2524, and AA2024 samples were revealed to contain a larger number of pits that were slightly larger in size in all three directions. Further examination of the microstructure and texture of both non-corroded and corroded samples via scanning electron microscopy will be presented, with careful examination of the role of secondary phases in influencing pitting potential.

Introduction

Design requirement for aircraft have become more and stricter with each passing generation [1]. These requirements include: high strength, corrosion resistance, reduced weight, high elastic modulus, reduced maintenance cost, and low manufacturing costs [1]. On top of all of these requirements, recent mandates by the government and environmental agencies are requiring the usage of chromate free coating systems on all aerospace systems. The needs of the aerospace community must be addressed by corrosion engineers to come up with coating systems that can be applied to high strength aluminum alloy to provide an adequate level of corrosion protection while maintaining the material parameters needed for advanced aircraft design.

Currently, the state of the art for aerospace design has been to use incumbent alloys like 2024 and 7075 are not adequately protected by the chromate free coatings available. While much research is being done on developing better coating systems and surface pre-treatments [2-4] are

being researched, there has not been a single solution that has solved the issue of chromate coatings. If a coating system cannot be created to solve all of the problems posed by corrosion, then working with a more corrosion resistant alloy, like aluminum-lithium-copper alloy AA2099, may be able to be used with the chromate free coating systems.

The attractiveness of alloys like AA2099 is that alloying with lithium 3 wt. % decrease in density per 1 wt.% of lithium added, 6% increase in elastic modulus per 1 wt.% lithium added, and lithium additions assist with the formation of precipitate strengthening phases [5]. Specifically, the aluminum-lithium-copper systems of alloys feature as good or better mechanical properties than incumbent alloy 2024 [6]. The most important consideration with these alloys is that improved corrosion resistance, higher than that of 7xxx and 2xxx series, is achieved by Zn additions in the aluminum lithium alloy system [5]. This makes this alloy system ideal for further analysis of its corrosion behavior as compared to traditional high strength aluminum alloys [7].

The aim of this work is to elaborate on the relationship between the microstructure of traditional and modern high strength aluminum alloys, specifically the role of second phase particles, and the corrosion response of the material. This will be achieved by using salt spray cabinet exposures to determine performance of five different alloys systems: AA2024-T3, AA2524-T3, AA7075-T6, AA7050-T6, and AA2099-T3. These alloys will be evaluated for pit number density and cumulative pit distribution by optical profilometry, with the observations made by this technique coupled with optical microscopy results.

Experimental Setup

The aluminum alloys and their nominal compositions are shown in Table 1. All materials were obtained from corrosion materials suppliers. All samples, with the exception of AA2099-T3 and AA2524-T3 plate, had samples taken from the longitudinal, longitudinal-transverse, and

short-transverse plate directions. AA2099-T3 had samples taken from the longitudinal and short-transverse directions only. AA2524-T3 was considered to be the longitudinal direction only. AA2024-T351, AA2099-T3, and AA7075-T6 samples cut into rectangles and were of the size of 1 in by 1 in by 0.39 in (2.54 cm by 2.54 cm by 1 cm). AA2524-T3 and AA7050-T6 samples were cut in a similar manner to the larger samples and measured .5 in by .5 in by 0.39 in (1.27 cm by 1.27 cm by 1 cm). Thickness of AA2524-T3 samples was restricted to the thickness of the plate, .16 in (.41 cm).

Table 1: Nominal Compositions of Alloys Tested

	Cu	Zn	Li	Mg	Mn	Fe	Si	Cr	Al
2024-T3	4.4	0.1	0.0	1.3	0.6	0.2	0.1	0.0	93.0
2524-T3	3.8	0.0	0.0	1.2	0.5	0.06	0.13	0.0	94.0
2099-T3	2.5	0.6	1.6	0.2	0.3	0.03	0.10	0.0	95.0
7075-T6	1.5	5.1	0.0	2.3	0.0	0.18	0.05	0.2	91.0
7050-T6	2.1	5.8	0.0	2.1	0.0	0.1	0.06	0.01	90.0

All samples were polished with SiC grinding papers in water until a finish of 4000 grit was reached. This finish was chosen to ensure that the secondary phase particles could be easily seen. Samples were rinsed in ethanol after each grinding step to assist in keeping the surface free of contaminates between each grinding step. After all grinding steps were completed, samples were cleaned ultrasonically in ethanol to ensure the removal of all contaminates to the surface before sample exposure. Samples were then attached via superglue or double sided tape to plastic cards to allow for exposure in an ASTM B117 salt spray cabinet.

Testing Methods

Samples were exposed to ASTM B117 salt fog tests for 72 hours, 120 hours, and 168 hours. Conditions for the ASTM B117 salt spray chamber technique are 95 °F (35°C), 100% relative humidity, with a 5 wt. % NaCl fog solution [8]. Samples exposed in the salt fog chamber were mounted in plastic racks at an angle of 30-45 degrees to expose the sample surface, as shown in Figure 1. Two samples from each side of the aluminum alloy (longitudinal, longitudinal-transverse, short-transverse) were exposed for each exposure condition. After exposure, samples were removed from the chamber and cleaned ultrasonically with a 25-30 vol. % nitric acid cleaning solution until the surface of the sample remained constant during solution exposure, approximately three minutes.

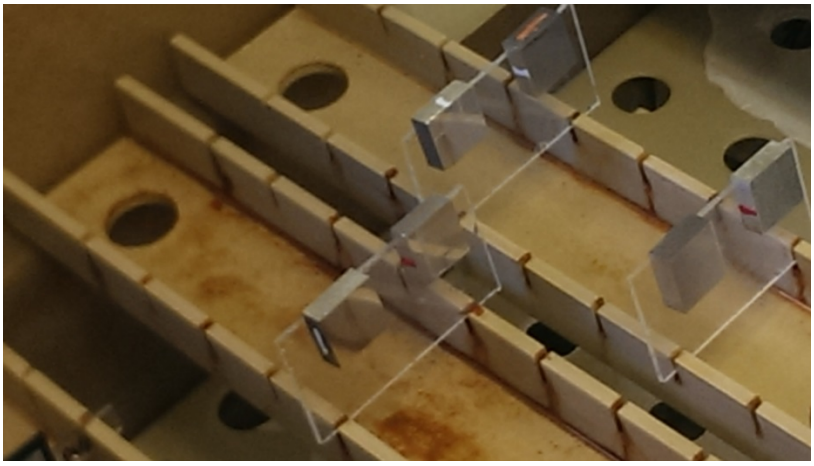

Figure 1: Example of Sample Set Up in Environmental Chamber

After cleaning, samples were inspected visually to determine any difference in surface condition after exposure. Samples were also examined using optical microscopy with focus on the condition of the remaining secondary phase particles. Unexposed and etched samples of each alloy were also prepared using a weakened Keller's etchant and examined by optical microscopy to expose the micro-structure of the alloy prior to exposure.

Exposed samples were also examined by optical profilometry to examine the depth and number of pits that formed during exposure to ASTM B117 environment. Profilometry was performed on the samples under the conditions of VSI mode, white light, with a 5x lens and 2x multiplier, making the system effectively operate at a 10x magnification. Sample scans were of a size of 1200 microns by 900 microns with various backscan values based on surface condition, but the length of each scan was fixed at 4000 microns to ensure that most pit depths could be established. The threshold for the data was set at 2% for all scans. All post processing was performed with Bruker's Vision 64 software [9] to determine the pit depths, with pits with depths between 20 microns and 1500 microns considered valid due to the limitation of the technique.

Due to the condition of the surface, the method of how pit depths were obtain will be explained here. Since a true reference surface could not be obtained because of generalized corrosion and left over corrosion product from the cleaning process, a reference surface was determined from the optical profilometry data based on the location of uncorroded material. After correcting for all tilt factors, the profilometry data was examined for a region of uncorroded material, with the depth values associated with that region of material used to formulate an average value for the reference surface. This value was used to determine pit depth values for the scan in question.

Results and Discussion

Visual Inspection

Analysis of the surfaces of the samples after cleaning by the nitric acid solution was invaluable to discovering the differences in corrosion behavior between the five alloys studied. Images of the samples are presented in Table 2. It is apparent that the surface of the samples changes depending on the alloy and exposure conditions. All samples except 2099-T3 featured a

difficult to remove corrosion product on the surface of the sample after cleaning. It should be noted that AA7050 and AA2524 featured less corrosion product remaining after nitric acid cleaning. This may be related to the fact that these alloys are to feature less large particles, like AA2099.

The corrosion product on the surface for AA7075 was the most difficult to remove corrosion product, with the resulting residue forming a dark brown product obscuring parts of the surface. 2024-T3 and 2524-T3 corrosion product was easier to remove, with the resulting corrosion residue retaining a whitish color on the sample surface. In contrast, AA2099-T3 had almost all corrosion product removed from the surface of the sample after cleaning, with only a slight film on the sample surface remaining.

The differences in the surface conditions of the sample after removal of the corrosion product speak to the differences in corrosion behavior of each sample. AA2099-T3 does not form such a rough, difficult to remove corrosion product on exposure to an adverse environment, indicating that this alloy has a different corrosion response than the other alloys. It is well known in the literature that precipitates in aluminum –lithium-copper alloys are smaller than those found in other high strength aluminum alloys [5] . This provides fewer sites for attack, which would provide fewer sites to generate corrosion product. The corrosion product composition may also play a role in the difference between 2099-T3 and the other alloys tested, but this has to be further researched.

Optical Microscopy

Optical microscopy was performed on the samples to examine the effects of exposure to the salt spray environment on the sample surface in more detail. Images of the samples before exposure to corrosion are shown in Figure 2. 2024-T3 and 7075-T6 feature large intermetallic

particles arranged in stringers as well as strong rolling texture. These two microstructures also feature larger grains that the other alloys tested. 2424-T3 and 7050-T6, which are cleaner versions of 2024 and 7075, respectively, feature less large particles than their predecessors, but the microstructures are still quite complex. In contrast to the other alloys, 2099-T3 features a much less complex microstructure with smaller particles and smaller grain.

The complexity of the microstructure, specifically the arrangement and size of the secondary phase particles, has proven to be important to determining the corrosion behavior. As seen in Figure 3, corrosion attack originates on the secondary phase particles present in the matrix. For 2024-T3 and 7075-T6, the large particles arranged in stringers lead to pit coalescence as the particles are dissolved during corrosion attack. In all cases for these two alloys, for the longitudinal-transverse and short-transverse directions were seen to exhibit areas of localized corrosion. The large size of the particles also leads to increases in pit depths, as will be shown by optical profilometry. These same behaviors were observed in the cleaner 2524-T3 and 7050-T6 alloys, but to a lesser degree due to the relative cleanliness of the alloy as compared to the incumbent alloys.

In stark contrast to the behavior of the older generation of high strength aluminum alloys, is the modern alloy 2099-T3. Due to the simplicity of the microstructure and the small size of the particles s observed in alloys like 2099, the sites available for corrosion attack are minimized and localized corrosion is abated. While the corrosion behavior of this alloy is driven by the various intermetallics strengthening phases distributed throughout the microstructure [10, 11], the size and special distribution of the particles leads to lessened corrosion attack and lessened ability to have pit coalescence during exposure. The small size of the anodic particles lead to small pits distributed throughout the matrix that are quite shallow and seem to stop growing in

size once the particle has been dissolved. The special separation between the pits along with their small size prevents many of the pits from coalescing, although some pit coalescence has been observed. Due to this factor, it makes sense that no localized corrosion would be observed in the longitudinal-transverse and short-transverse sides of the alloy.

Optical Profilometry

Examination of the samples exposed to salt spray chamber by optical profilometry revealed a link between the sample microstructure and pitting behavior. As previously stated in the discussion about the optical microscopy of the alloys studied, larger secondary phase particles seemed to produce larger pits than smaller secondary phase particles. This behavior is observed in the analysis of the cumulative pit distributions seen in Figure 4. As exposure time is increased, the pit depth distributions for all alloys except for 2099 tend to increase. This signifies that pit depths are becoming deeper as the large secondary phase particles are being dissolved away. Since the pit depth distribution for 2099-T3 does not increase significantly with time, it can be determined that the pit growth for this alloy with respect to time is halted due to the alloys lack of large particles. Once the particles are dissolved away, there are few sites left for corrosion attack to occur, so the alloy suffers less corrosion damage than the older high strength aluminum alloys.

This is hypothesis is confirmed with the examination of the pit number density for each alloy during the 72 hour, 120 hour, and 168 hour exposure period. Pit number densities for AA2099 remain consistently lower than the other alloys tested. The only other alloy that had a similar pit number density was AA2024, but this was not due to the alloys corrosion resistance. The low pit number density can be explained by the large, deep pits that tended to form from the

Table 2: Results for the Visual Inspection of Samples Tested for 72 and 120 Hours in B117

	120 Hour Test	72Hour Test
2024-T3		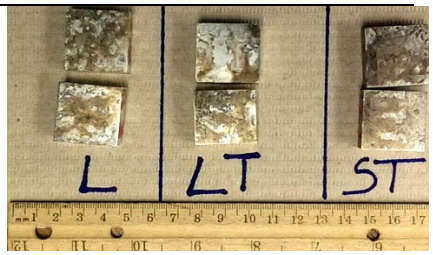
2524-T3	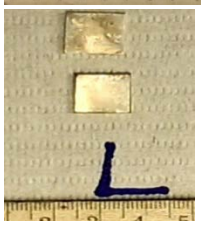	
2099-T3	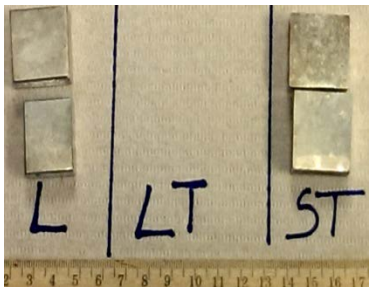	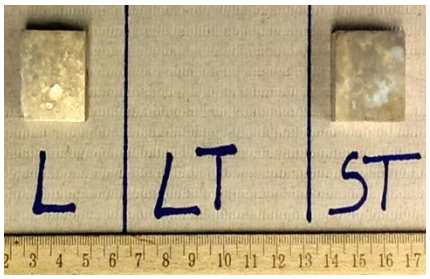
7075-T6		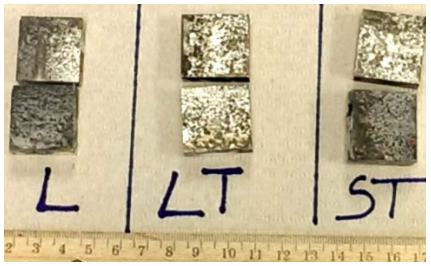
7050-T6		

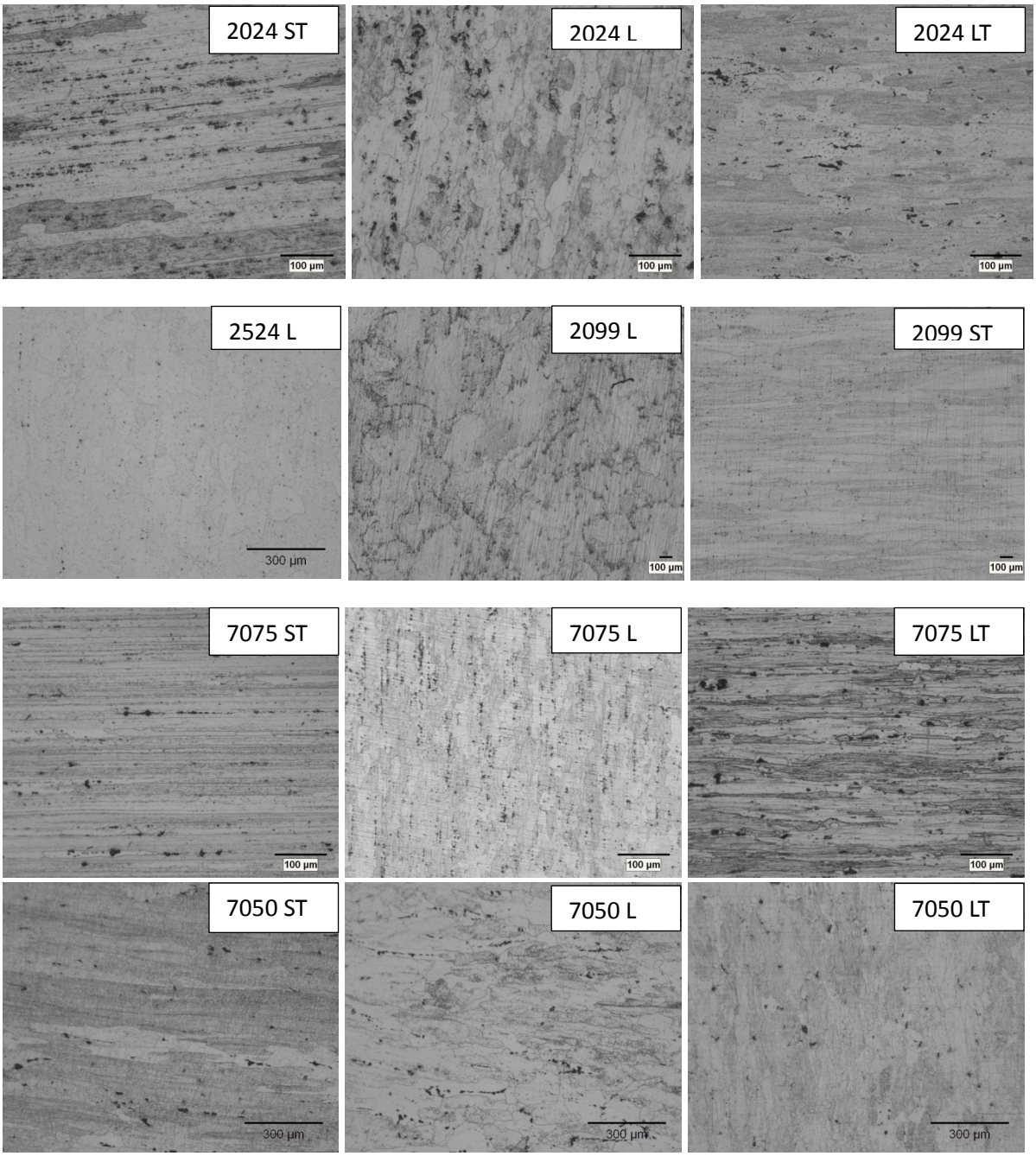

Figure 2: Uncorroded and Etched Images of All Alloys Tested. AA2099 images feature a less complicated microstructure than other the other alloys, leading to less corrosion attack.

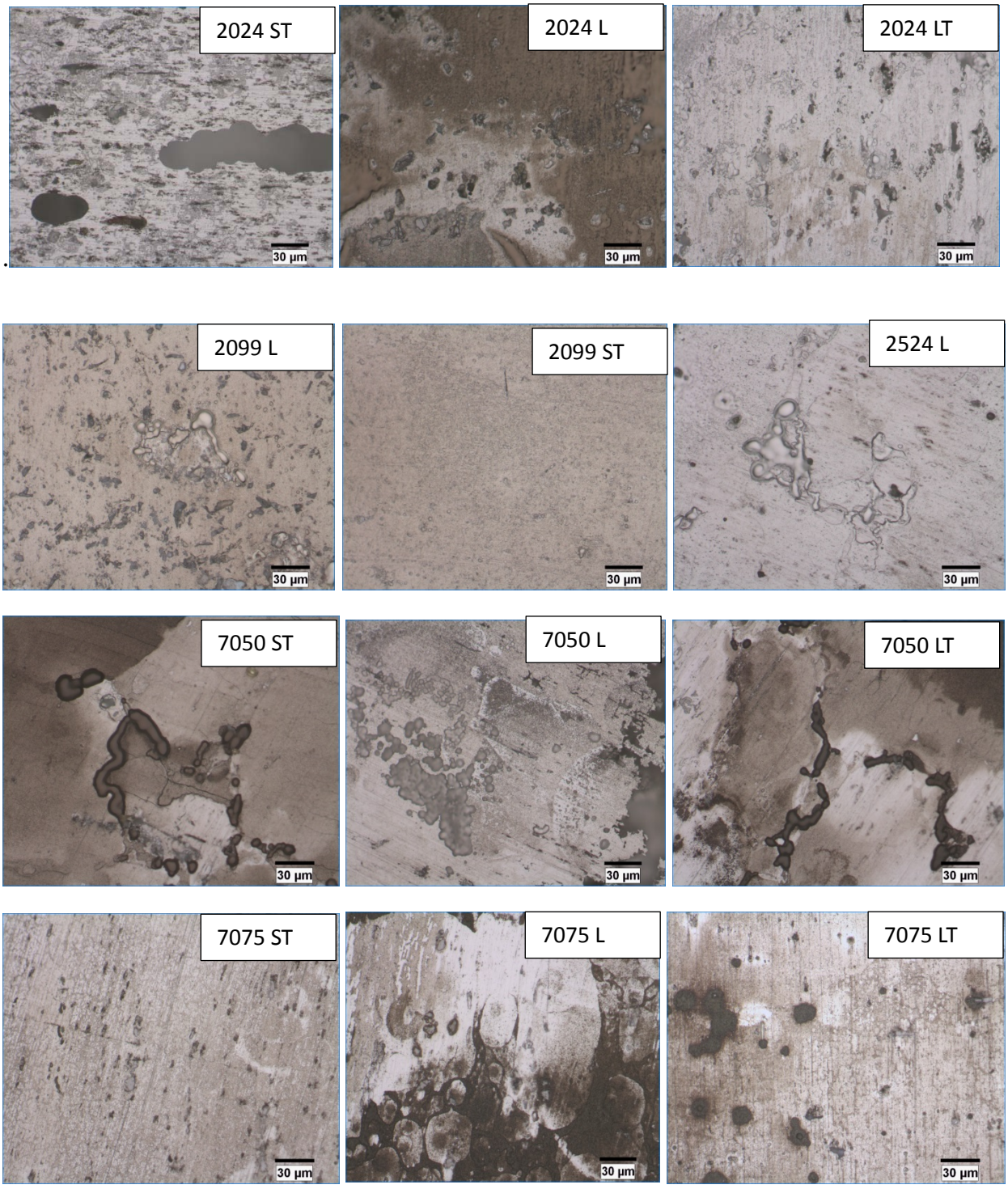

Figure 3: Images of the Samples after Corrosion Exposure of 72 Hours. Corrosion attack can be seen to occur around secondary phase particles. Larger pits are observed on samples that feature larger secondary phase particles.

corrosion attack. These pits would coalesce, so the total number of pits in the alloy would

decrease as the size of the pits increased.

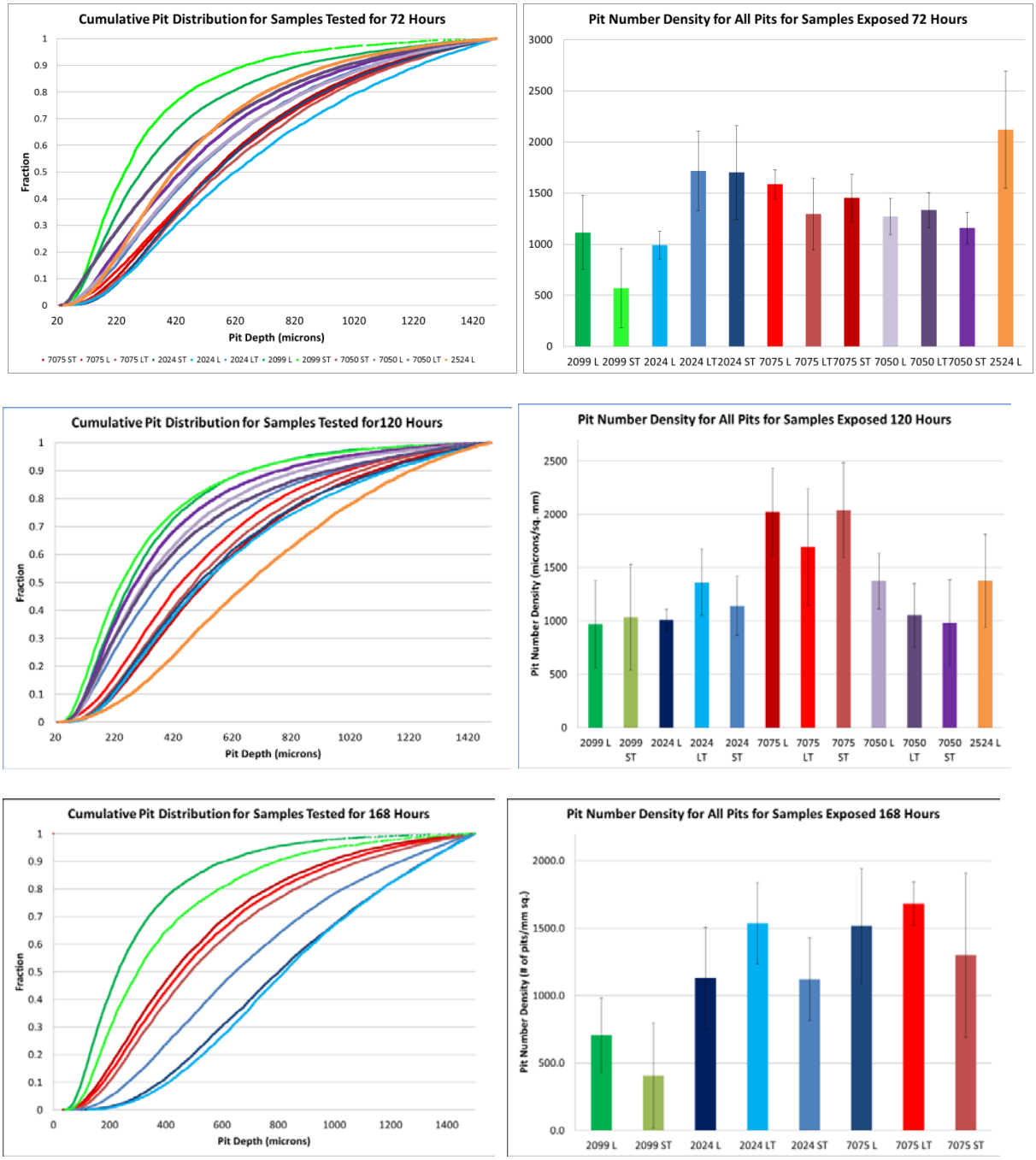

Figure 4: Cumulative Pit Depths and Pit Number Density Graphs for the Exposed Samples. AA2099 consistently has a more shallow pit distribution than the other alloys tested, which is attributed to the smaller secondary phase particles in the alloys microstructure

AA7075 and AA7050 behaved as expected, with high pit number densities due to the large number of secondary phase particles in the alloy causing the pit number densities to be higher. AA7050 seemed to be the most corrosion resistant of the traditional alloys, which was expected as the alloy features a much cleaner microstructure than the others. The behavior of AA2524 was surprising, in that the microstructure was supposed to be cleaner than that of AA2024. The high pit number densities may be attributed to the fact that this sample was a sheet sample rather than plate, but more work on this is needed.

Summary

Optical profilometry of the samples exposed to ASTM B117 salt spray demonstrated the strong effect of microstructure on the corrosion response of the alloys tested. As expected, the cleaner microstructure of AA2099 yielded generally a lower pit number density and cumulative pit distribution than all other alloys for each time exposure. This result was due to the smaller particles found in the alloy microstructure, as seen by the optical microscopy. Larger particles, as observed in the more traditional high strength alloys, resulted in deeper pits that often coalesced to form extremely large pits, which was demonstrated in the optical profilometry data as high pit number densities and deeper cumulative pit distributions. Visual inspection of the alloys demonstrated that the corrosion product formed on the surface may also be affected by the cleanliness of the microstructure, as AA2099, AA2524, and AA7050 featured less corrosion product on the surface after cleaning.

Acknowledgments

The authors acknowledge the help of the Ohio State University Department of Materials Science machine shop for all help with sample machining, Anthony Lutton for assistance with trace element analysis of the alloys used in this work, and Steve Bright for assistance with sample

preparation and etching. The authors acknowledge that this research is sponsored by the U.S. Air Force Academy under agreement FA7000-12-2-0015.

References

[1] J. Liu, Materials Science Forum, 519-521 (2006) 1233-1238.
[2] S. Lin, H. Shih, F. Mansfeld, Corrosion Science, 33 (1992) 1331-1349.
[3] Y. Ma, X. Zhou, G.E. Thompson, M. Curioni, T. Hasimoto, P. Skeldon, P. Thomson, M. Fowles, Journal of The Electrochemical Society, 158 (2011) C17-C22.
[4] Y. Ma, X. Zhou, G.E. Thompson, M. Curioni, X. Zhong, E. Koroleva, P. Skeldon, P. Thomson, M. Folwes, Corrosion Science, 53 (2011) 4141-4151.
[5] R.J. Rioja, J. Liu, Metallurgical and Materials Transactions A, 43A (2012) 3325-3337.
[6] C. Giummarra, B. Thomas, R.J. Rioja, in: Light Metals Technology Conference, 2007, pp. 6.
[7] J.P. Moran, E.A. Starke Jr., G.E. Stoner, J. G.L. Cahen, Corrosion, 43 (1987) 374-382.
[8] A. International, in, ASTM International, West Conshohocken, PA, 2011, pp. 12.
[9] in, Bruker, 2012.
[10] C. Kumai, J. Kusinski, G. Thomas, T.M. Devine, Corrosion, 45 (1989) 294-302.
[11] R.G. Buchheit, J.P. Moran, G.E. Stoner, Corrosion, 50 (1994) 120-130.